Development of an Efficient Multi-Reach Partitioning Approach with Linear Muskingum Method and Weighted Mean of Vectors Algorithm for Inverse Flood Routing

Maziar Rastegarfar [1], Ali Raeisi Isa-Abadi [2,*], Hamed Reza Zarif Sanayei [1]

1. Department of Civil Engineering, Shahrekord University, Shahrekord, Iran.
2. Department of Water Engineering, Shahrekord University, Shahrekord, Iran.

***Corresponding Author:**
Ali Raeisi Isa-Abadi

Email: ali_raeisi@sku.ac.ir
Received: 2025.11.26
Accepted: 2026.02.10
J. Hydraul. Struct., 12(3):70-93
DOI: 10.22055/jhs.2026.51239.1369

ABSTRACT

This study presents an inverse routing method based on the linear Muskingum model, utilizing a new and efficient optimization algorithm i.e., the weIghted meaN oF vectOrs (INFO) to determine optimal routing parameters. Additionally, the analyzed rivers are segmented into smaller intervals, then the linear Muskingum routing method is applied separately and consecutively to each interval. Furthermore, lateral flow contribution has been integrated into the calculation process to improve routing accuracy in the linear Muskingum method. It is worth noting that this study is novel in two key aspects: it is the first to apply a partitioning approach to an inverse flood routing strategy, and, more broadly, across all types of flood routing—whether inverse or direct—it marks the first instance in which the number of sub-reaches has been optimized within an inverse Muskingum flood routing framework, while simultaneously estimating routing parameters and accounting for lateral flow effects. The proposed Muskingum model is investigated on three flood events, and its performance is compared to existing methods reported in the literature. The sum of squared errors (SSQ) significantly decreases for each analyzed flood event, with best SSQ values of 167.03 for the triangular flood hydrograph, 371.55 for the Wilson data, and 128.63 for the double-peak hydrograph. Also, the Standardized Absolute Deviation (SAD) evaluation criteria, yielding best SAD values of 194.17, 70.03, and 45.83 for the respective events, along with the visual agreement of observed input hydrographs and the resulting routing hydrographs, highlight the advantages of the proposed method.

KEYWORDS
Inverse Flood routing, linear Muskingum method, INFO, optimization algorithms, Multi-reach.

1. Introduction

Flood routing is conducted in direct and inverse modes. Inverse routing determines the upstream hydrograph characteristics based on the specifications of the downstream hydrograph. It provides valuable insights into upstream inflow flood characteristics, which are crucial for estimating reconstruction and renovation costs associated with upstream flooding. Additionally, it assists in determining the appropriate volume of water to release from a regulation dam to meet downstream flow requirements. Furthermore, inverse routing can be employed to validate data from upstream hydrometric stations.

Muskingum method is based on continuity and storage equations and can be implanted using both linear and non-linear models [1]. Due to the high computational costs for calibration, the non-linear models are recommended primarily when discharge and storage equations exhibit non-linearity [2]. On the other hand, the linear Muskingum equation is not only simpler but also more cost-effective than non-linear Muskingum methods. Consequently, this approach has been extensively utilized in variety of researches.

Samani and Shamsipour [3] proposed a model using the linear Muskingum method (LMM) for flood routing in multi-branch rivers. They employed a non-linear optimization method to estimate the required parameters. Al-Humoud and Esen [4] presented two approximate methods for estimating linear Muskingum model parameters. In the first method, it was essential to calculate the slopes of both the inflow and outflow hydrographs at the intersection point, as well as the maximum storage volume within that region. In contrast, the second method required the calculation of the inflow and outflow hydrographs at only two specific points.

In order to estimate the parameters of the Muskingum method, Ayvaz and Gurarsian [5] presented a new model which can be applied to all flood routing programs Their results showed that proposed model significantly enhances the performance of the Muskingum method. Bazargan and Norouzi [6] utilized the LMM for Molasani and Ahvaz hydrometry stations located upstream and downstream of the Karun River. They demonstrated that the accuracy of this method can be improved by using variable values instead of constant parameters for X, K, and Δt, particularly at the peak of hydrograph. Norouzi and Bazargan [7] estimated the parameters of a linear model for two major floods, as opposed to just one, in eight different models. Their findings indicated that by applying the arithmetic mean values of X and K, along with the geometric mean value of Δt related to two significant floods, they attained improved accuracy in estimating the peak section of the downstream hydrograph. Omran et al. [8] employed Muskingum's graphical method along with numerical methods to conduct flood routing. The improved bat algorithm (IBA) was also used in that study to optimize the estimated values of the Muskingum model. Results indicated that all numerical methods could estimate the parameters of Muskingum's graphical method, but the IBA was the best method as it fits data with minimum errors. In a research [9], the parameters of the Muskingum model were optimized to accurately simulate hourly flood hydrographs for three rivers within the Karun watershed. The researchers assessed the model's performance using the correlation coefficient (CC), the ratio of the root-mean-square error to the standard deviation of measured data (PSR), Nash–Sutcliffe efficiency (NSE), and index of agreement (d). The findings demonstrated that the gray wolf optimization (GWO) algorithm provided superior performance in simulating floods in the study area. Salvati et al. [9] combined the nonLMM with a new lateral flow equation based on five decision variables to perform flood routing more accurate. In a research conducted by Mohsenabadi [10], a Multilinear Muskingum method was developed specifically for D-shape cross-section and compared against the Saint-Venant model. This research focused on optimizing discharge coefficients to obtain water surface profiles. Results indicated a suitable agreement between routed hydrographs and water surface profiles.

Although there have been extensive studies in the field of the Muskingum model for direct flood routing, its application for inverse flood routing remains limited. Inverse flood routing was first performed by Eli et al. [11] on the James River in Virginia using the Saint-Venant equations. They noted numerical instabilities, particularly at low discharges. Das [12] presented the inverse routing method for the

Muskingum model using Lagrange multipliers for optimizations. A study by Koussis et al. [13] , applied the Muskingum method for inverse flood routing and observed that input hydrographs were estimated with good accuracy. In another research, Hosseini Dehnoi [14] used Genetic Algorithm (GA) to define the inverse LMM in multi-branch rivers. The algorithm proved to be accurate and effective in generating artificial data rather than real data. Badfar et al.[15] developed a new model for inverse flood routing based on the Muskingum model. They used the Euler numerical and Runge-Kutta fourth order methods to solve the storage function while the Shuffled Complex Evolution (SCE) algorithm was employed for parameters optimization.

To achieve accurate results in flood routing, it is essential to estimate the Muskingum parameters optimally. Due to the complexity of these calculations, various methods, including metaheuristic optimization algorithms, have been introduced over the years. Mohan [16] applied Genetic Algorithm (GA) for estimating parameters in linear and non-linear models. Results illustrated that using GA was more appropriate than previous methods and initial assumption close to optimal solution was not required. Moghadam et al. [17] examined the application of all linear and non-linear Muskingum models using Particle Swarm Optimization (PSO) algorithm. Ultimately, the most appropriate Muskingum model was selected based on evaluation criteria comparing observed and computed discharges. Badfar et al. [18] utilized Shuffled Complex Evolution (SCE) algorithm to optimize Muskingum parameters. Their results indicated that the algorithm performs well and shows good agreement between computed and observed hydrographs in simulating floods. In another research, RezapourTabari and Emami Dehcheshmeh [19] proposed a novel structure for the non-linear Muskingum model. A combination of Particle Swarm Optimization (PSO) and Dove Swarm Optimization (DSO) metaheuristic algorithms were used for optimization of parameters. Norouzi et al. [20] utilized data from four floods in the Karun River to optimize flood routing using the PSO algorithm. In their research, the LMM parameters were separately optimized and applied to compute outflow hydrographs for each flood.

Considering the limited knowledge and studies in the literature on inverse flood routing using the Muskingum method along rivers, it is essential to conduct research in this field. Therefore, the current study develops a linear Muskingum model for multi-reach inverse routing in several flood-prone rivers. Also, given the need to obtain optimal values for effective parameters in this area, the weIghted meaN oF vectOrs (INFO) algorithm is utilized to optimize LMM parameters and determine the optimal number of ranges. INFO is a new and powerful algorithm, that has not been widely used in different fields of water engineering. It is worth mentioning; the multi-reach method constitutes a novel approach proposed in this research. Furthermore, the investigation of lateral discharge has been conducted in this study to enhance the accuracy of computational outcomes.

2. Materials and methods

2.1. Inverse flood routing approach

The current study applies the linear Muskingum method for inverse flood routing, incorporating two fundamental equations: the continuity and the linear storage equations. The continuity equation (Eq. 1) states that the variation in storage volume over time is equal to the difference between inflow and outflow. Also, the storage equation (Eq. 2) establishes a linear relationship between the storage volume and the inflow and outflow rates,

$$\frac{dS}{dt} = (1+\beta)(I-O) \quad (1)$$

$$S = K[X(1+\beta)I + (1-X)O] \quad (2)$$

where I and O represent inflow and outflow rates, respectively, S corresponds the total water storage volume, X is a dimensionless weighting factor that indicates the relative importance of inflow (I) and outflow (O) in relation to the storage volume (S). Acceptable values of X range between 0 and 0.5, as values exceeding 0.5 result in an unrealistic increase in flood peaks, while negative values are considered practically meaningless for the weighting factor [21] . K represents the storage time constant and depends on factors such as channel length and flood wave celerity. The value of K is approximately equal to the time required for the flood to pass through the river. The parameter β represents the coefficient or contribution of lateral flow with respect to the inflow, which may vary along the river, either increasing or decreasing [22].

In inverse flood routing, unlike the direct procedure, the inflow rate at the beginning of a time step is the unknown variable to be determined. Therefore, by applying Eqs. (1) and (2) over a time interval of length Δt, with indices 1 and 2 representing values at the beginning and end of the time step, respectively, the upstream discharge at the start of the time step can be computed using the following equation:

$$I_1 = C_1 O_2 + C_2 O_1 + C_3 I_2 \tag{3}$$

Where C_1, C_2, and C_3 are obtained as follows:

$$\begin{aligned} C_1 &= \frac{1}{(1+\beta)} \frac{K(1-X)+\theta\Delta t}{KX+(1-\theta)\Delta t} \\ C_2 &= -\frac{1}{(1+\beta)} \frac{K(1-X)-(1-\theta)\Delta t}{KX+(1-\theta)\Delta t} \\ C_3 &= \frac{KX-\theta\Delta t}{KX+(1-\theta)\Delta t} \end{aligned} \tag{4}$$

where θ is a parameter used to weight the average of the inflow/outflow (I/O) values at the beginning and end of each time step. Knowing the parameters K and X, the coefficients C_1, C_2, and C_3 can be computed. The value of I_1 in Eq. (3) can be determined using the outflow at the beginning and end of the time step, along with the inflow at the end of the time step. This process can then be iterated in reverse through successive time steps until the upstream hydrograph is completely calculated. It is important to emphasize that the derivation of Eqs. (3) and (4) to perform inverse flood routing while incorporating lateral discharge constitutes a key innovation presented in this study.

2.2. Multi-reach LMM in inverse flood routing

To improve the accuracy of the proposed flood routing procedure, a multi-reach version is also introduced. The term "multi-reach" refers to the division of the river reach into two or more sub-reaches (Fig. 1). Consequently, the flood routing procedure can be applied separately to each sub-reach, successively following the completion of the previous one. It should be noted that, since the proposed approach is a lumped model, the spatial location and manner in which the river reach is divided into sub-reaches are entirely unimportant. The only aspect that matters is the number of divisions. This is why the sub-reach lengths are shown as equally spaced in Fig. 1.

In general, the flood routing procedure begins from the last sub-reach (most downstream), proceeds upstream, and ends at the first sub-reach (most upstream). Using the outflow hydrograph for each sub-reach and applying Eq. (3), the corresponding inflow hydrograph can be determined. Note that, except for the last sub-reach where the outflow data is known (from the observed hydrograph at the downstream end of the river), the outflow data for the remaining sub-reaches is unknown and needs to be determined. By using the computed inflow hydrograph as the outflow hydrograph for the subsequent upstream sub-reach, this issue is effectively resolved. Thus, this iterative procedure should begin with the last sub-reach and continue until reaching the first one.

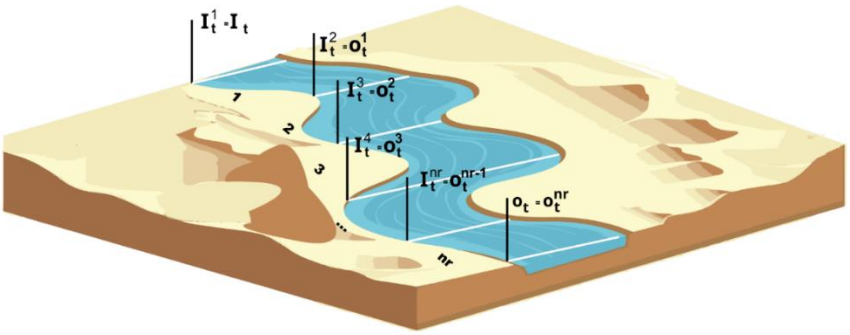


Figure 1. Multi-reach LMM in inverse routing

It should be noted that the Muskingum parameters are assumed constant in all reaches. While these parameters can be varied in every sub-reach, considering uniform parameters in the presented study reduces the number of decision variables and minimizes uncertainties associated with parameter estimation. Moreover, to enhance the accuracy of routing computations, this study introduces the calculation of the optimal number of sub-reaches for a given river as a key decision variable, marking a novel contribution to the methodology as it has not been previously utilized in the literature. Therefore, in addition to K, X, and β, the number of sub-reaches (nr) is a new parameter in the proposed Muskingum model and must be determined. The optimization technique (INFO algorithm) is utilized to calculate the optimal values of these parameters.

2.3. INFO optimization algorithm

Ahmadianfar et al. [23] introduced a novel optimization algorithm, called weighted mean of vectors, which can aid the formation of a solid structure by modifying the weighted mean method and updating the location of vectors. INFO is a population-based algorithm that computes the weighted mean of set of vectors in search space. The population includes a set of vectors illustrating possible solutions. INFO algorithm finds solutions in multiple consecutive generations. This algorithm consists of the following main phases that we address in the context of a minimization problem.

Initialization phase*:*

A population of INFO vectors can be represented as $\boldsymbol{X}^{g,l} = \{\boldsymbol{x}_1^{g,l}, \boldsymbol{x}_2^{g,l}, \cdots, \boldsymbol{x}_D^{g,l}\}$, where $g = 0,1,2,\cdots,g_{max}$ denotes the generation number, D is the dimension of the search domain, and $l = 1,2,\cdots,N_p$ corresponds to the l^{th} vector of the current population. This algorithm uses a random methodology for generating the initial population of vectors ($\boldsymbol{X}^{0,l}$). In this stage, some major control parameters called weighted mean coefficient δ and scaling coefficient s are also introduced for the INFO [23].

Rule renewal phase:

In INFO, in contrast to other methods, a mean-based renewing rule is used to generate new vectors, increasing the convergence rate. Updating the rule operator increases population diversity during the search procedure and generates new vectors using the weighted mean of vectors. The mean-based rule consists of two terms and is defined as follows [23]:

$$Mrule = \sum_{i=1}^{2} \alpha_i \times MBW_i^{g,l},\ \alpha_1 = r,\ \alpha_2 = 1 - r \quad (5)$$

where r is a random value in the range [0,0.5]; $MBW_i^{g,l}$ is obtained as follows:

$$MBW_i^{g,l} = \delta \times \frac{\sum_{j=1}^{3} w_j^i \left(x_{a_j}^i - x_{a_{j+1}}^i\right)}{\varepsilon + \sum_{j=1}^{3} w_j^i} + \varepsilon \times rnd, \quad if \quad (j+1) > 3: x_{a_{j+1}}^i = x_{a_1}^i$$
$$w_j^i = \cos\left(\left[f\left(x_{a_j}^i\right) - f\left(x_{a_{j+1}}^i\right)\right] + \pi\right) \exp\left(-\frac{f\left(x_{a_j}^i\right) - f\left(x_{a_{j+1}}^i\right)}{\omega_i}\right) \quad (6)$$

$l = 1, 2, \cdots, Np$, $g = 1,2, \cdots, g_{max}$, $i = 1,2$ and $j = 1, \cdots, 3$

where f represents the objective function (OF), $\omega_i = \max\left\{f\left(x_{a_j}^i\right)\right\}_{j=1}^{3}$. The values of $\{a_j\}_{j=1}^{3}$ } depend entirely on which term (i =1 or i =2) in Eq. (6) is being calculated. If $i = 1$, they represent three distinct numbers between 1 and Np, randomly generated to select three different vectors from the population in the g^{th} generation. Conversely, if i =2, they correspond to the best, better and worst solutions, respectively. That is, $x_{a_1}^2 = x_{bs}^{g,l}$, $x_{a_2}^2 = x_{bt}^{g,l}$, and $x_{a_3}^2 = x_{ws}^{g,l}$, where x_{bs}, x_{bt}, and x_{ws} are, respectively, the best, better, and worst solutions and $l = 1, 2, \cdots, Np$, $g = 1,2, \cdots, g_{max}$. ε is a constant value with low quantity, rnd is a random value. The δ scale coefficient is obtained using, $\delta = 4(rand - 0.5)\exp\left(\frac{-4g}{g_{max}}\right)$, where g_{max} is the maximum number of generations. Finally, the two new vectors are achieved based on

$$z_1^{g,l} = x_1^{g,l} + s \times Mrule + C_{A1}$$
$$z_2^{g,l} = x_2^{g,l} + s \times Mrule + C_{A2} \quad (7)$$

where C_{A1} and C_{A2} are the convergence acceleration terms added for updating the rule operator. $s = 4(rand - 0.5)\exp\left(\frac{-4g}{g_{max}}\right)$ is the scaling factor and notably, when the parameter s takes on large values, the current position shifts away from the weighted mean of the vectors, promoting exploration. Conversely, smaller values of s encourage the current position to converge toward the weighted mean, enhancing exploitation.

Combining phase:

By combining the two newly generated vectors ($z_1^{g,l}$and $z_2^{g,l}$) from the previous step, a new solution ($u^{g,l}$) is obtained. Two random values are generated to combine the vectors. For a given l^{th} vector, the first random value determines whether its position is updated, while the second random value dictates how $z_1^{g,l}$ and $z_2^{g,l}$ are merged to create a unique new vector solution, denoted as $u^{g,l}$ (see [23], for more details).

Local search phase:

While the last two phases focus on both exploration and exploitation of the algorithm, this phase places greater emphasis on exploitation. This objective is achieved through the use of global location (x_{best}^G) and the mean-based rule (see Eq. 5). According to this operator, a new vector can be generated in proximity to x_{best}^G by a random value between 0 and 1 [23]. Fig. 2 depicts the flowchart of the INFO and the optimization process.

2.4. Estimation of parameters and optimization procedure

The proposed inverse flood routing procedure involves estimating the parameters K, X, β and nr. To determine these parameters, an optimization process is required. For this purpose, the INFO algorithm is employed, with the sum of squared deviations (SSQ) serving as the OF:

$$SSQ = \sum_{i=1}^{N} (\hat{I}_i - I_i)^2 \quad (8)$$

Fig. 3 illustrates the integration of the INFO algorithm with the inverse flood routing procedure to determine the optimal parameters values.

2.5. Evaluation criteria

To validate the efficiency of the INFO optimization algorithm and assess the impact of the multi-reach approach applied in inverse flood routing using the LMM, some evaluation criteria are employed.

1- Accuracy of optimization method: The accuracy of the optimization method can be evaluated using the sum of absolute difference (SAD) between observed inflow ($\hat{I}_i$) and calculated inflow (I_i) at i^{th} time, These metrics are defined as follows:

$$SAD = \sum_{i=1}^{N} |\hat{I}_i - I_i| \quad (9)$$

Where N is the number of recorded data.

Lower SAD value indicates a closer agreement between the calculated results and the observed data, demonstrating reduced calculation errors.

2- Magnitude of Flood Peak: The absolute deviation between the peak values of the observed inflow ($\hat{I}_i^{peak}$) and the routed inflow (I_i^{peak}), referred to as DPO, represents a criterion for assessing the magnitude of the peak inflow.

$$DPO = |\hat{I}_i^{peak} - I_i^{peak}| \quad (10)$$

The lower the DPO value, the closer the observed and calculated values are.

3- Mean absolute relative error: The mean absolute relative error (MARE) between the observed and calculated inflows is considered as:

$$MARE = \frac{1}{N}\sum_{i=1}^{N} \frac{|\hat{I}_i - I_i|}{\hat{I}_i} \quad (11)$$

A lower MARE value indicates a reduced average relative difference between the observed and calculated inflows, which implies better model accuracy and performance.

4- Variance: The similarity in the shape and size of the hydrograph can be quantified using the variance criterion (VarexQ), which is expressed as:

$$VarexQ = \left(1 - \frac{\sum_{i=1}^{N}(\hat{I}_i - I_i)^2}{\sum_{i=1}^{N}(\hat{I}_i - \hat{I}_i^{mean})^2}\right) \times 100 \quad (12)$$

Where $\hat{I}_i^{mean}$ is the mean observed inflow.

A higher $VarexQ$ value indicates greater similarity between the observed and calculated inflow hydrographs.

5- Coefficient of determination (R^2): The R^2 value quantifies the proportion of variance in the observed inflows that is explained by the calculated inflows. A value of R^2 =1 indicates perfect agreement between the observed and calculated inflows, while R^2=0 suggests no correlation.

$$R^2 = \frac{[\sum_{i=1}^{N}(\hat{I}_i - I_i)(\hat{I}_i^{mean} - I_i^{mean})]^2}{\sqrt{\sum_{i=1}^{N}(\hat{I}_i - I_i)^2 \sum_{i=1}^{N}(\hat{I}_i^{mean} - I_i^{mean})^2}} \quad (13)$$

Where I_i^{mean} is the mean calculated inflow.

6- The Kling-Gupta (KG) Efficiency coefficient: It is a criteria particularly used to evaluate the overall performance of hydrological models by considering multiple aspects of model accuracy, including correlation, variability, and systematic errors. It is defined as:

$$KG = 1 - \sqrt{(R-1)^2 + \left(\frac{\sigma}{\hat{\sigma}} - 1\right)^2 + \left(\frac{I_i^{mean}}{\hat{I}_i^{mean}} - 1\right)^2} \quad (14)$$

Where and $\hat{\sigma}$ and σ are standard deviations of observed and calculated inflow, respectively [24].

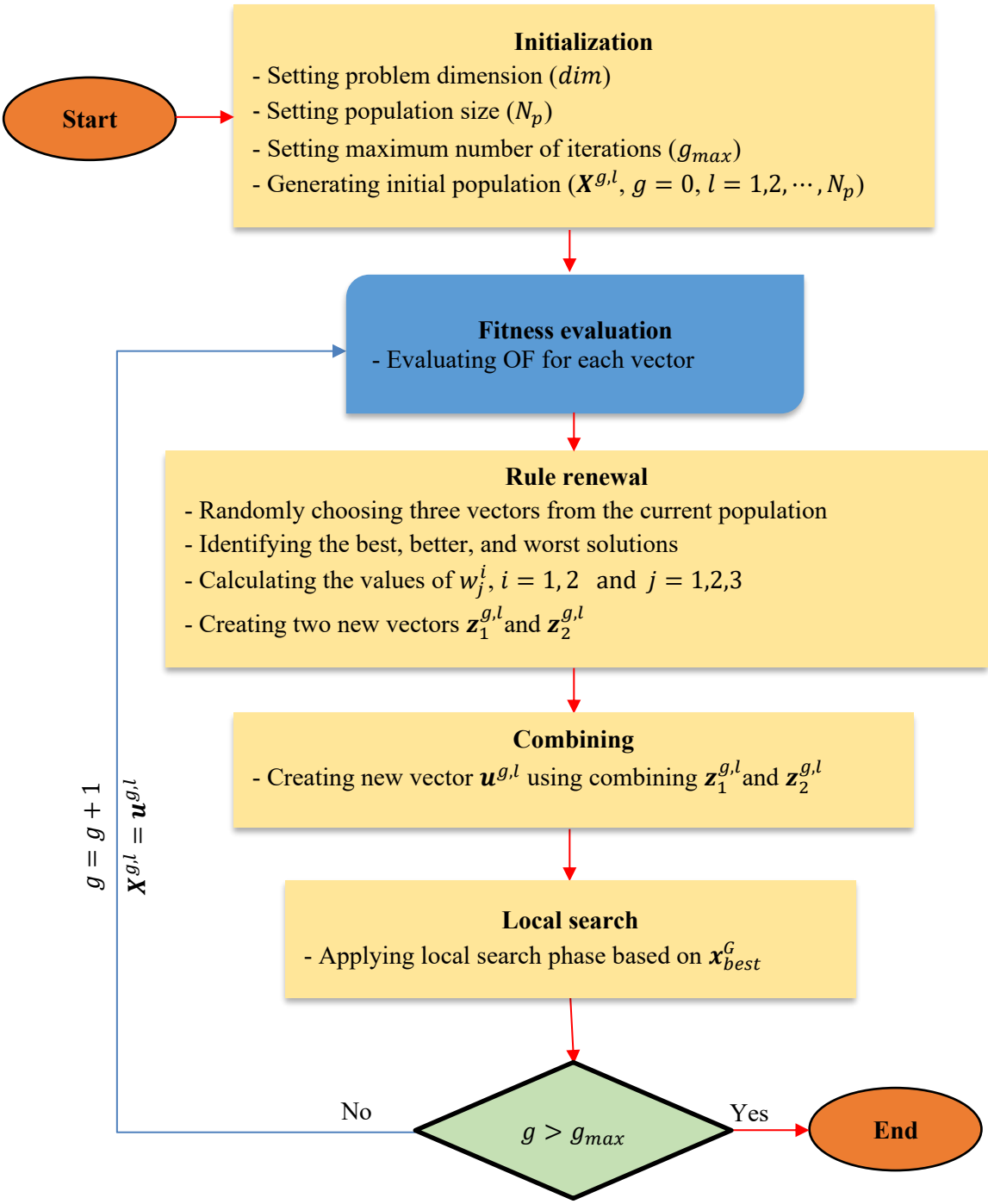


Figure 2. Flowchart of the weighted mean of vectors (INFO) algorithm

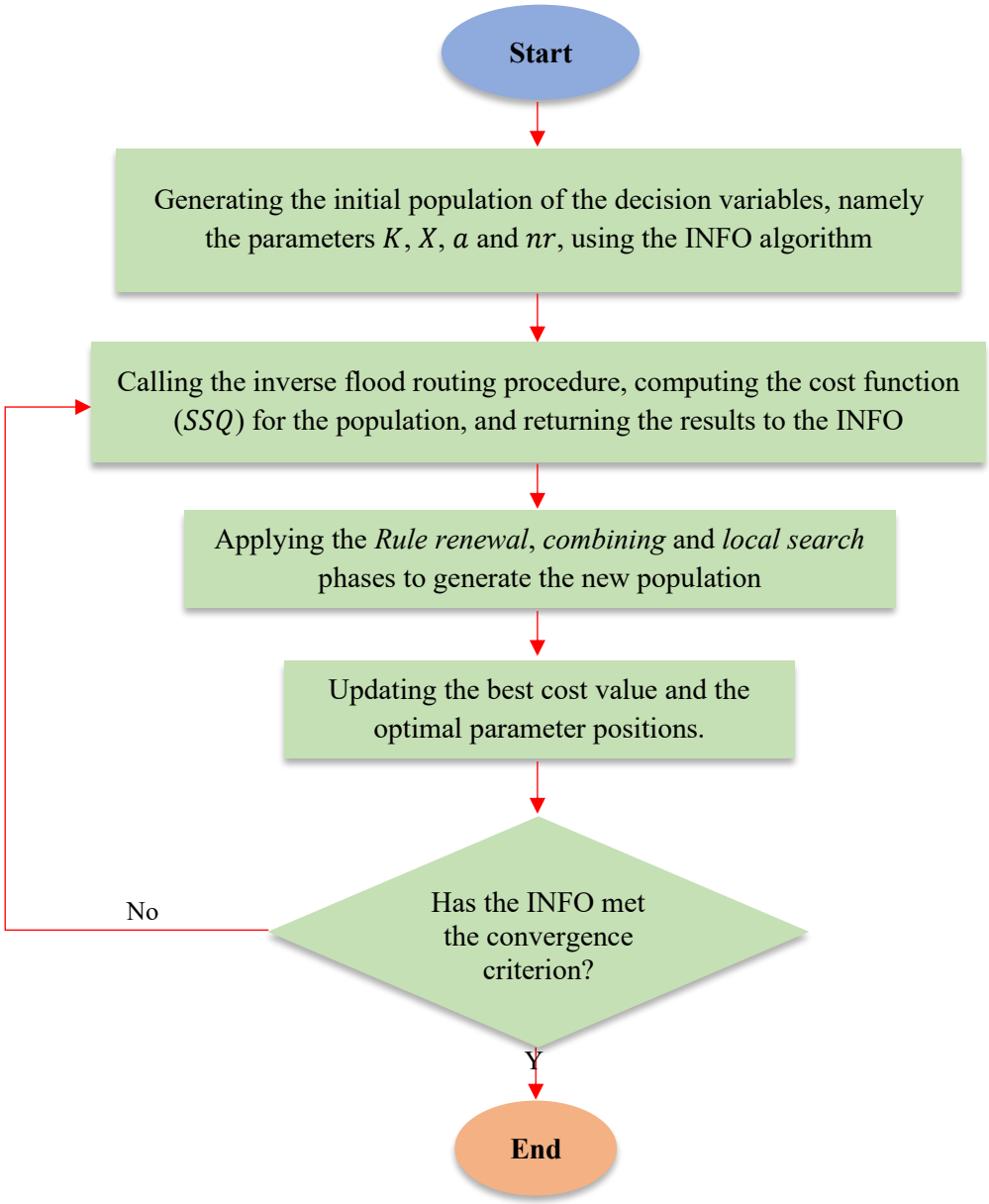


Figure 3. The process of determining the optimal parameter values through the integration of the INFO algorithm and the inverse flood routing procedure.

3. Results and discussion

The present study evaluates the performance of the proposed Muskingum method using triangular, single-peak, and double-peak flood hydrographs. The evaluation criteria computed in this research are compared with other established methods in the literature. To identify the optimal values of the decision variables in the Muskingum method and ensure rapid convergence during optimization, the following parameter ranges are considered: $0 < X < 0.5$, $0 < K < 60$, $-1 < \beta < 1$. Additionally, the parameters for the INFO algorithm employed across all experiments are specified as follows: N_p=30, dim=4, and g_{max}=2000.

According to the reported flood data, the analysis includes 43-time steps, with each time step having a duration of 3 hours (N = 43, Δt = 3).

Fig. 4 illustrates the convergence process of the INFO optimization algorithm in determining the decision variables of the triangular flood hydrograph. As shown, the algorithm begins with a randomly generated initial solution, which is inaccurate, and iteratively reduces the OF value to achieve an optimal solution.

The optimal parameter values for both the single- and multi-reach LMMs, along with the corresponding optimal value of nr, are presented in Table 1. For each number of partitions (nr), the reported Muskingum

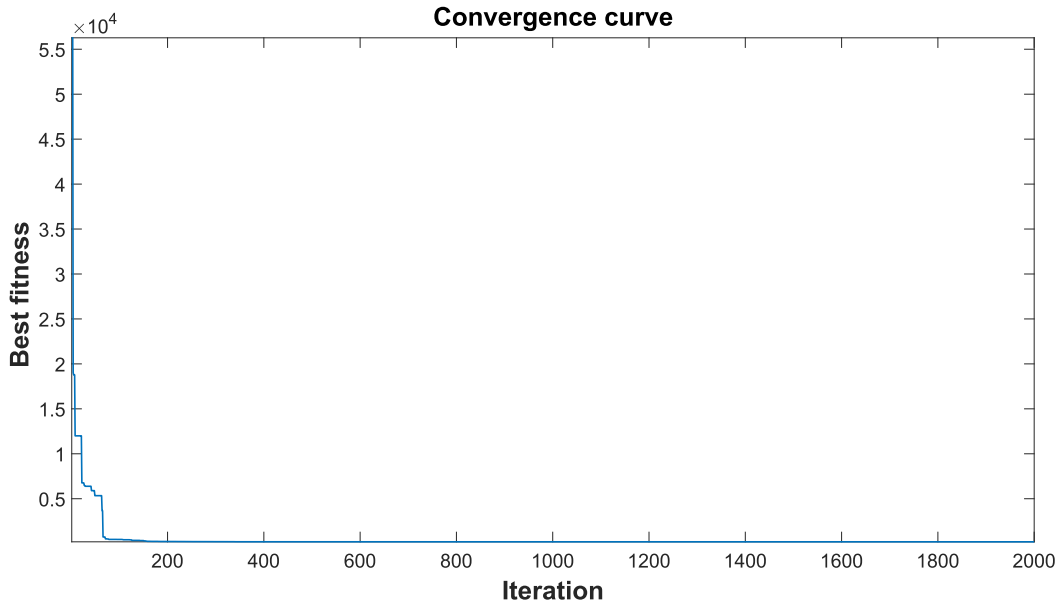


Figure 4. Convergence procedure of multi-reach Muskingum parameters by INFO algorithm for triangular flood data

3.1. Triangular flood hydrograph

A synthetic triangular inflow hydrograph within a rectangular channel with a length of 4500 m, a surface width of 60 m, a surface slope of 0.01, and a Manning coefficient of 0.035 is utilized in this study. The flood demonstrates a linear relationship between the storage volume rate and the difference between inflow and outflow, making it a suitable case for evaluating the proposed method in this study [25]. parameters (K, X, β) represent effective values for the entire multi-reach system. Table 2 presents the inverse-routed flood hydrograph at the river upstream in comparison to the observed flood data. As demonstrated, the obtained results exhibit a strong agreement with the observed data, highlighting the accuracy and reliability of the proposed method.

Saghafian et al. [25] utilized the triangular hydrograph data to validate their

suggested method. They applied the kinematic wave method with a 3-minute time step for simulating the upstream hydrograph. Similarly, Badfar et al. [15] used the triangular hydrograph data for inverse routing by LMM incorporating Euler numerical models and the fourth-order Runge-Kutta method for time discretization. To enhance the accuracy of the results, they employed the Shuffled Complex Evolution (SCE) algorithm to define the Muskingum parameters. Fig. 5 illustrates the inverse-routed inflow hydrograph using the INFO optimization algorithm, compared with the observed upstream hydrograph. The results from Saghafian et al. [25] and Badfar et al. [15] are also superimposed. As shown, the hydrograph obtained using the proposed approach is smoother and demonstrates good agreement with the observed data, whereas the inflow hydrograph calculated by Saghafian et al. [25] exhibits significant fluctuations in flow value.

To quantitatively compare the proposed method in the current study with the results of Saghafian et al. [25] and Badfar et al. [15] , evaluation criteria are presented here (see Table 3). As can be concluded, the results of the suggested method are more accurate than those of the two other studies. The SSQ, SAD, and DPO are the common evaluation criteria used across all studies. These three metrics consistently demonstrate that the proposed approach outperforms previous methods without exception. Specifically, the SSQ value shows significant improvement—by 64% and 31% compared to the studies of Saghafian et al. [25] and Badfar et al. [15] , respectively. This indicates the effectiveness and strength of INFO in minimizing the SSQ, highlighting its applicability and benefits in achieving optimal solutions in flood routing problems.

Table 1- Optimal parameter values of single- and multi-reach LMM for the triangular flood data

Method	X	K(h)	β	nr
Single-reach	0.1993	3.1794	0.0033	-
Multi-reach	0.18	5	-0.52	4

Table 2-The results of the suggested inverse flood routing procedure for the triangular hydrograph

	Observed hydrograph		Routed hydrograph
Time (hr)	Inflow (m^3/s)	Outflow (m^3/s)	Inflow (m^3/s)
0	54	54	54.19
3	54	54	54.40
6	54	54	54.83
9	54	54	55.69
12	57	54.05	57.15
15	60	54.25	59.36
18	63	54.68	62.53
21	69	55.51	66.67
24	75	56.88	71.77
27	81	58.92	77.70
30	87	61.74	84.21
33	93	65.35	91.11
36	99	69.71	98.20
39	105	74.72	105.34
42	111	80.28	112.39
45	117	86.24	119.30
48	123	92.49	126.02
51	129	98.92	132.46
54	135	105.47	138.42
57	141	112.06	143.55
60	147	118.67	147.02
63	153	125.27	147.68
66	147	131.29	145.39
69	141	135.97	140.81
72	135	138.8	134.90
75	129	139.66	128.45
78	123	138.75	121.91
81	117	136.41	115.54
84	111	133	109.41
87	105	128.86	103.48
90	99	124.21	97.77
93	93	119.26	92.20
96	87	114.11	86.78
99	81	108.86	81.48
102	75	103.55	76.37
105	69	98.23	71.51
108	63	92.92	67.01
111	60	87.71	62.82
114	57	82.69	58.77
117	54	77.96	53.94
120	54	73.61	53.51
123	54	69.73	53.99
126	54	66.37	54.00

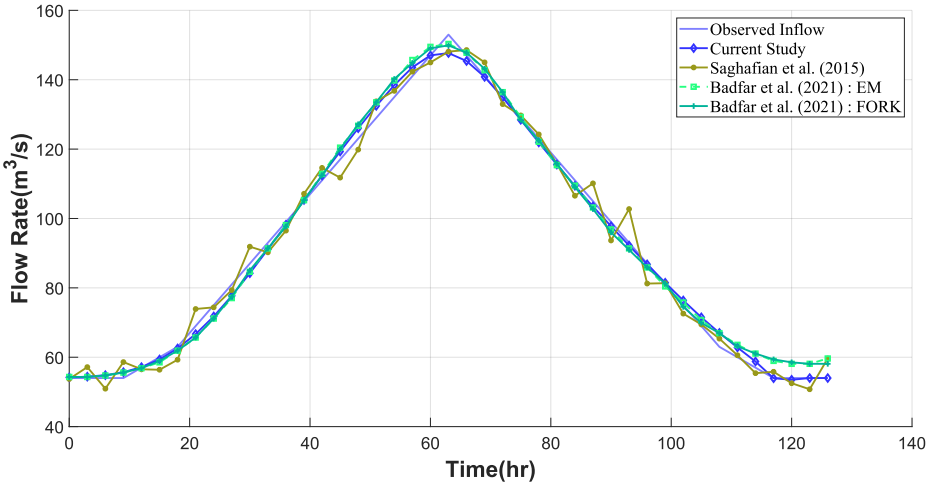


Figure 5. The routed inflow hydrograph in comparison with those of Saghafian et al. [25] and Badfar et al. [15] for the triangular flood data

Table 3. Muskingum methods evaluation criteria for the triangular flood data

Criterion	Badfar et al. [15]		Saghafian et al. [25]	Current Study			
	EM	*FORK*		$nr = 1$	$nr = 2$	$nr^* = 4$	$nr = 6$
SSQ	280	280	534.0943	194.1718	186.6469	**167.0303**	271.3878
SAD	89	89	864	73.7901	71.7206	64.3682	86.0992
$MARE$	-	-	-	0.0203	0.0197	0.0169	0.0255
DPO	3.0	3.0	8.9	4.6214	4.88	5.3158	6.2463
$VarexQ$	-	-	-	99.5685	99.5852	99.6288	99.3669
R^2	-	-	-	0.9957	0.9959	0.9963	0.9940
KG	-	-	-	0.9963	0.9964	0.9965	0.9958

* Optimal

It should be noted that increasing the number of sub-reaches does not necessarily lead to improved accuracy. Therefore, the results for the optimal number of sub-reaches are also compared with those obtained from non-optimal subdivisions and the undivided (single-reach) case, as shown in Table 3 and Fig. 6. As detailed, the most accurate solutions correspond to the optimal number of sub-reaches (i.e., *nr* = 4). Interestingly, the worst results are not associated with the undivided case (*nr* = 1), but rather with the scenario involving the highest number of subdivisions (*nr* = 6). This outcome highlights the effectiveness of the proposed optimal dividing approach. Figure 6 further supports this conclusion, as the optimized multi-reach scenario shows a closer alignment with the observed flood data compared to the other methods.

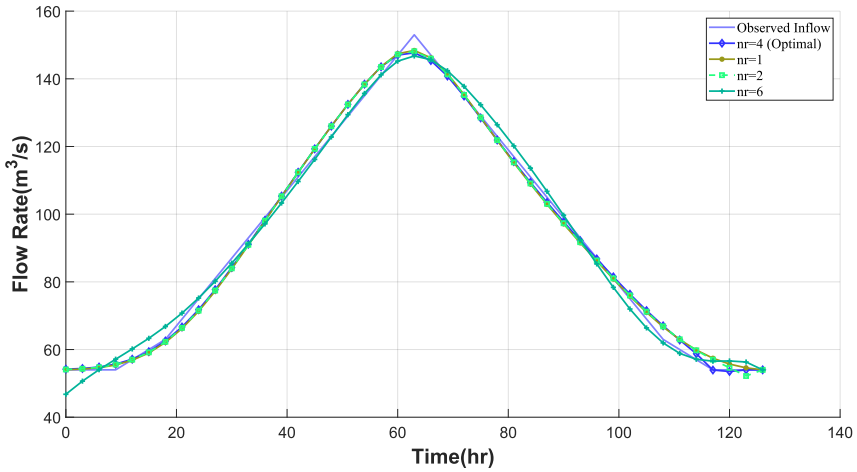


Figure 6. Comparison of routed inflow hydrographs for optimal and non-optimal sub-reach configurations, based on triangular flood data

3.2. Wilson flood data

Wilson flood represents one of the most important datasets, with extensive applications in the evaluation of flood routing models. It has been employed as a benchmark problem in many researches [26]. The dataset consists of 21 time steps (N=21), with each time step representing a 6-hour interval (Δt =6 hr).

The routing procedure was configured and executed for this flood event, and the multi-reach LMM parameters were subsequently obtained using the INFO. Fig. 7 indicates the INFO convergence process for the single-peak Wilson hydrograph data. The algorithm begins with an initial random solution and iteratively reduces the objective function (OF) value until it reaches the optimal solution.

Table 4 presents the optimized parameters obtained for both the single-reach and multi-reach cases, along with the corresponding optimal value of nr. Table 5 demonstrates the inverse-routed flood results compared to the observed upstream flood data. As shown, the obtained routing results exhibit a good agreement with the recorded flood values, highlighting the accuracy and reliability of the proposed method.

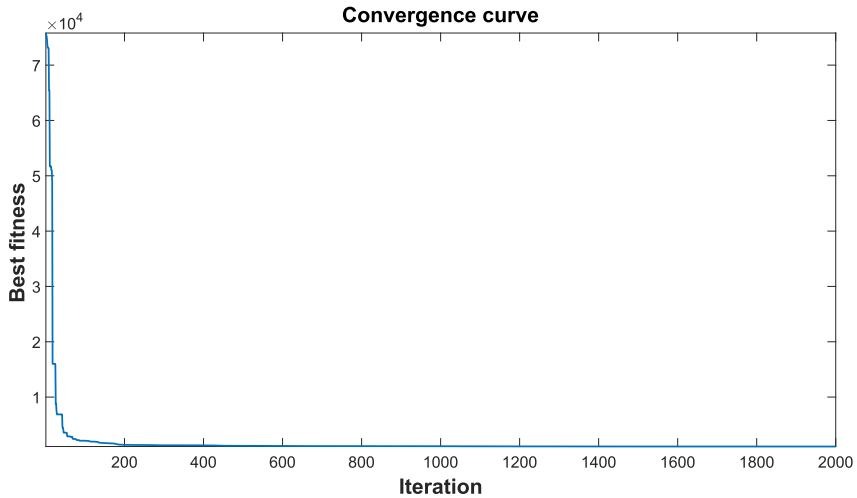


Figure 7. Convergence procedure of multi-reach Muskingum parameters by INFO algorithm for single-peak flood data (Wilson data)

Table 4. Optimal parameter values of single- and multi-reach LMM for the single-peak flood data (Wilson data)

Method	X	K (h)	β	nr
Single-reach	0.2403	15.7065	-0.023	-
Multi-reach	0.3542	23.84	-0.0042	9

Table 5. The results of the suggested inverse flood routing procedure for the single-peak hydrograph

	Observed hydrograph		Routed hydrograph
Time (hr)	Inflow (m^3/s)	Outflow (m^3/s)	Inflow (m^3/s)
0	22	22	23.70
6	23	21	14.74
12	35	21	44.17
18	71	26	75.86
24	103	34	97.27
30	111	44	106.53
36	109	55	105.89
42	100	66	98.58
48	86	75	87.60
54	71	82	75.18
60	59	85	62.85
66	47	84	51.54
72	39	80	41.70
78	32	73	23.51
84	28	64	26.98
90	24	54	22.02
96	22	44	18.51
102	21	36	16.33
108	20	30	15.44
114	19	25	15.81
120	19	22	17.55
126	18	19	18.00

Das [12] utilized this data for inverse flood routing by applying linear and non-linear Muskingum methods and minimized the difference between observed and calculated inflows. The inverse-routed flood hydrograph for the Wilson data, derived using the proposed method, was compared with the observed hydrograph and the results reported by Das [12] and Badfar et al. [15] (see Figure 8). As shown, the results closely match the observed data in terms of both peak value and timing of occurrence, whereas the results reported by Das [12] and Badfar et al. [15] show a lower peak value and a delayed peak time compared to the observed data.

Table 6 also compares the evaluation criteria of the suggested method with those of Das [12] and Badfar et al. [15] . The results indicate that the proposed method produced more accurate and reliable outcomes compared to the alternatives. Specifically, the SSQ value achieved by the INFO was reduced by 37% in undivided case compared to the models used in the study by Das [12] . Also, comparison the values of SAD and DPO criteria with those of Das [12] and Badfar et al. [15] , again shows the superiority of the proposed approach.

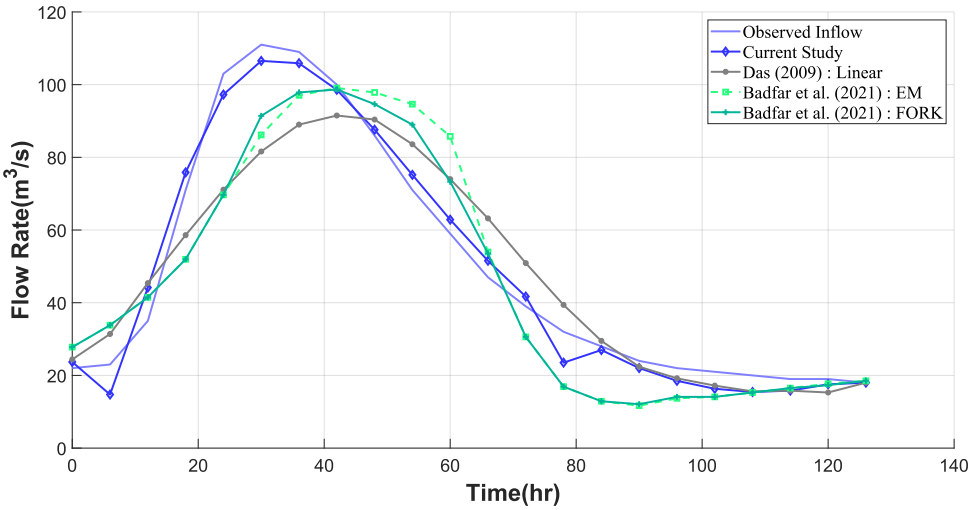


Figure 8. The routed inflow hydrograph in comparison with those of Das [12] and Badfar et al. [15] for the single-peak flood data (Wilson data)

Table 6. Muskingum methods evaluation criteria for the single-peak flood data (Wilson data)

Criterion	Badfar et al. [15]		Das [12]	Current Study			
	EM	*FORK*		*nr=1*	$nr = 7$	$nr^* = 9$	$nr = 11$
SSQ	2311	2237	3624	2301.947	1137.8618	**371.5487**	592.4724
SAD	190	184	212	180.0253	116.3485	70.0253	87.4099
$MARE$	-	-	-	0.414	0.1337	0.0908	0.1078
DPO	12.5	12.4	19.5	11.62	7.3719	0.96	1.2429
$VarexQ$	-	-	-	90.2348	95.1730	98.4238	97.4866
R^2	-	-	-	0.9043	0.9517	0.9843	0.9749
KG	-	-	-	0.9483	0.9706	0.9818	0.9793

Table 6 presents a comparison of the results based on single and multiple reach subdivisions. As shown, the optimal number of subdivisions for the Wilson data was found to be 9, leading to a reduction in the SSQ value by more than threefold compared to the undivided (single-reach) case. Moreover, the SSQ for this configuration is over 1.5 times lower than that for the 11-subdivision case. Figure 9 illustrates the flood routing results for the single-peak flood data, comparing the accuracy of the single-reach, non-optimal multi-reach, and optimal multi-reach (nr = 9) configurations. As shown, the routed flood in the optimized multi-reach configuration demonstrates a closer agreement with the observed flood compared to the other cases. This observation is further supported by the data in Table 6, where the SSQ and SAD values for the optimized multi-reach state are lower than those corresponding to the non-optimal number of subdivisions.

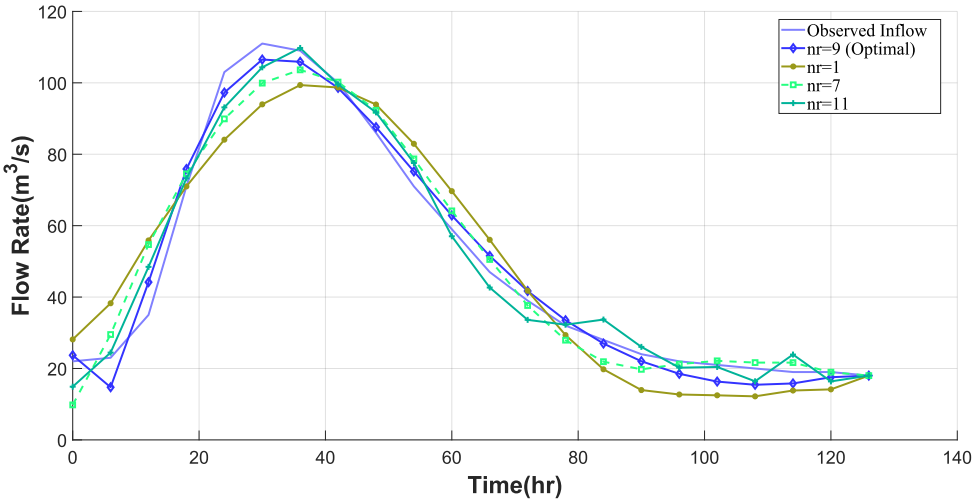


Figure 9. Comparison of routed inflow hydrographs for optimal and non-optimal sub-reach configurations, based on single-peak flood data (Wilson data)

3.3. Double-peak hydrograph

Saghafian et al. [25] investigated a double-peak hydrograph within a rectangular channel that measured 4,500 meters in length, had a top width of 50 meters, a bed slope of 0.01, and a Manning roughness coefficient of 0.025. This flood demonstrated a linear relation between storage volume and weighted flow [15]. In the reported data for this flood, the number of time steps is 25, and the length of each time step is 3 hours (N=25, $\Delta t = 3$).

Fig. 10 illustrates the convergence process of the INFO optimization algorithm for determining decision variables in multi-reach case for the double-peak hydrograph. As observed the algorithm initiates with a random starting solution and progressively minimizes the target function value, ultimately reaching an optimal solution. The parameters obtained from the optimization process in both single- and multi- reach cases, as well as the optimal value of nr are given in Table 7. Table 8 compares the inverse-routed inflow hydrograph with the observed one. As shown, there is strong agreement between the routed and recorded flood data, indicating a high level of accuracy in the proposed inverse flood routing process.

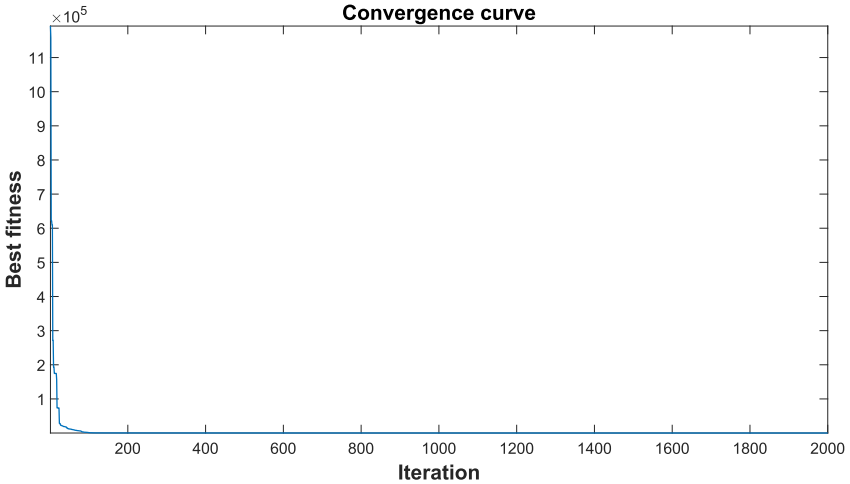


Figure 10. Convergence procedure of multi-reach Muskingum parameters by INFO algorithm for double peak flood data

Table 7. Optimal parameter values of single- and multi-reach LMM for the double-peak hydrograph

Method	X	K(h)	β	nr
Single-reach	0.1862	11.7351	0.034	-
Multi-reach	0.351	2.054	-0.0063	5

Table 8. The results of the suggested inverse flood routing procedure for the double-peak hydrograph

	Observed hydrograph		Routed hydrograph
Time (hr)	Inflow (m^3/s)	Outflow (m^3/s)	Inflow (m^3/s)
0	150	150	149.16
3	150	150	150.65
6	163.33	150.64	164.46
9	191.67	153.56	193.19
12	235	161.4	231.50
15	268.33	176.01	267.37
18	285.67	196.57	288.42
21	287	219.3	288.56
24	272.33	238.97	270.80
27	250	251.4	244.93
30	220	254.68	224.76
33	216.67	251.04	217.54
36	223.33	244.61	223.40
39	240	239.35	236.95
42	251.33	237.37	251.29
45	258	238.79	260.14
48	260	242.43	258.18
51	243.33	245.58	245.70
54	225	245.79	226.30
57	205	241.9	204.11
60	185	233.98	182.71
63	166.67	222.92	164.97
66	150	209.83	153.79
69	150	196.51	148.76
72	150	184.49	150.00

Saghafian et al. [25] employed the double-peak flood hydrograph data to validate their proposed method. They applied the kinematic wave method to simulate the upstream hydrograph, utilizing a time interval of three minutes. Figure 11 illustrates the inverse-routed flood hydrograph in comparison with the observed hydrograph and the results reported by Saghafian et al. [25]. As observed, the hydrograph presented by Saghafian et al. [25] exhibits several fluctuations, while the hydrograph generated using the proposed approach closely aligns with the observed hydrograph, particularly in terms of both the

magnitude and timing of the two observed peaks. In addition, the rising and recession limbs of both peaks in the routed hydrograph align closely with those of the observed hydrograph. The results are also compared with those of Badfar et al. [15] in Fig. 11, where double-peak flood data were used for inverse flood routing using the linear Muskingum method. As illustrated, the calculated inflow hydrograph demonstrates a closer match to the observed hydrograph than the one presented by Badfar et al. [15].

Further details of these comparisons, along with the evaluation criteria, are provided in Table 9. The results presented in this table show that the proposed methodology in this research provides more accurate and reliable outcomes compared with the other evaluated methods. Overall, it can be noted that the kinematic wave method by Saghafian et al. [25] exhibited the lowest level of accuracy, whereas the suggested method achieved the highest accuracy. The proposed model in the present study also exhibits improved performance in terms of the SSQ and SAD criteria when compared to the models of Saghafian et al. [25] and Badfar et al. [15]. Notably, the SSQ value was reduced by approximately 40% relative to the findings of Saghafian et al. [25] , and by about 15% compared to the results reported by Badfar et al. [15].

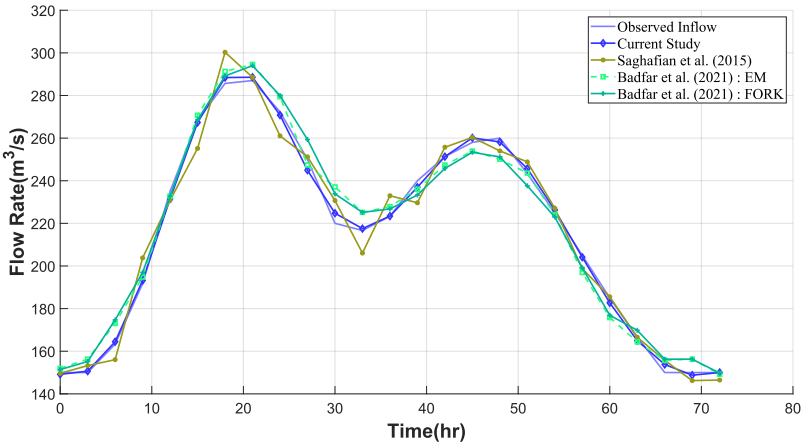


Figure 11. The routed inflow hydrograph in comparison with those of Saghafian et al. [25] and Badfar et al. [15] for the double-peak flood data

Table 9. Muskingum methods evaluation criteria for the double-peak flood data

Criterion	Badfar et al. [15]		Saghafian et al. [25]	Current Study			
	EM	*FORK*		$nr = 1$	$nr = 3$	$nr^* = 5$	$nr = 7$
SSQ	967	967	1368	823.463	310.5111	**128.6247**	642.3044
SAD	124	124	858	118.8228	72.6080	45.8292	98.5738
$MARE$	-	-	-	0.0216	0.0133	0.0086	0.0202
DPO	7.6	7.6	45.6	4.9376	5.7623	1.566	1.7782
$VarexQ$	-	-	-	98.4287	99.4075	99.7545	98.7744
R^2	-	-	-	0.9844	0.9942	0.9975	0.9878
KG	-	-	-	0.9881	0.9905	0.9909	0.9891

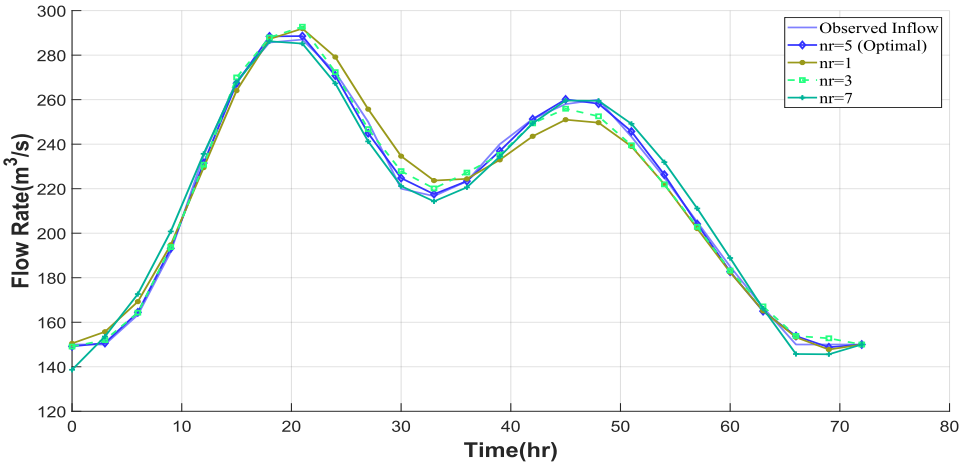


Figure 12- Comparison of routed inflow hydrographs for optimal and non-optimal sub-reach configurations, based on double-peak flood data

Figure 12 presents the results of flood routing using the single-reach LMM, along with the optimized and unoptimized multi-reach LMM, applied to the double-peak flood data. As shown, the routed hydrograph in the optimized multi-reach case aligns more closely with the observed flood compared to the other configurations. This observation is further supported by the SSQ and other evaluation criteria values presented in Table 9. As described, a significant reduction in the SSQ value was observed when $nr = 5$, the identified optimal number of sub-reaches.

3.4. Additional insights

This section examines the impact of the number of subdivisions on model performance across different examples. Figure 13 presents the variation of the SSQ value relative to the optimal configuration for the triangular flood hydrograph, Wilson flood data, and the double-peak flood hydrograph, as a function of the number of subdivisions. Among these, the triangular flood hydrograph exhibits the smallest increase in SSQ when the number of subdivisions deviates from the optimal value, compared to the other two cases.

For the triangular flood hydrograph, the response to changes in the number of sub-reaches is notably asymmetric (Figure 13). When the number of sub-reaches is below the optimal value, the SSQ increases moderately—by up to 16% for $nr = 1$. In contrast, exceeding the optimal number leads to a substantial rise, with the SSQ increasing by as much as 233% at $nr = 8$. This highlights two key insights: first, increasing the number of sub-reaches does not necessarily improve model accuracy, contrary to common assumptions; and second, the model exhibits lower sensitivity to the number of subdivisions when fewer sub-reaches are used.

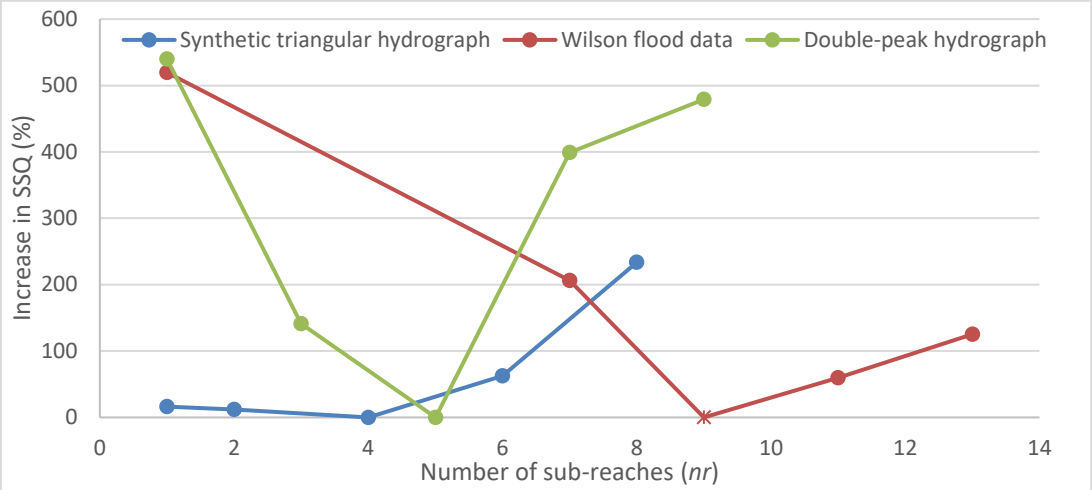


Figure 13. Percentage of increase in SSQ relative to optimal nr with varying the number of subdivisions in the three flood hydrograph cases

For the Wilson flood data, the variation in SSQ is also asymmetric; however, the increase in SSQ is more pronounced when the number of sub-reaches is less than the optimal value, compared to when it is greater than the optimal. Specifically, the SSQ increases by up to 520% for suboptimal subdivisions and by approximately 125% for over optimal subdivisions. This indicates that applying a single-reach LMM to the Wilson flood data results in significant inaccuracy relative to the optimal number of sub-reaches, and overall, this flood case is highly sensitive to the chosen subdivision level.

In the case of the double-peak flood data, the SSQ variations are nearly symmetric, with increases reaching up to 500%. This demonstrates that the double-peak flood is also highly sensitive to the number of sub-reaches selected for the proposed multi-reach LMM flood routing procedure.

4. Conclusion

In this study, a multi-reach Linear Muskingum Model (LMM) was employed for inverse flood routing, aiming to reconstruct the upstream inflow hydrograph based on downstream flow data. To estimate the parameters of the multi-reach LMM, the weighted mean of vectors (INFO) algorithm—a powerful meta-heuristic optimization technique—was utilized. Two strategies were adopted to enhance routing accuracy: (1) the contribution of lateral flow along the river was incorporated, and (2) the number of sub-reaches was treated as a decision variable and estimated alongside other model parameters.

The proposed multi-reach LMM integrated with INFO was tested using three distinct flood hydrographs: a triangular flood hydrograph, the Wilson flood data, and a double-peak flood hydrograph. The results were compared with those from previous studies. Even in the single-reach case, the proposed approach demonstrated higher accuracy across the three flood scenarios. When the number of sub-reaches was also optimized, the improvement became more significant; for example, in the double-peak case, the SSQ value was reduced by more than six times compared to the single-reach (no subdivision) state. Other evaluation metrics consistently confirmed the superior performance and robustness of the proposed method. Additionally, the analysis showed that the double-peak flood hydrograph is the most sensitive to the number of sub-reaches, whereas the triangular flood is the least sensitive. In conclusion, the developed multi-reach LMM with INFO proves to be an effective and reliable tool for inverse

flood routing. Future work could explore its application using a nonlinear Muskingum model to further enhance modeling capabilities.

Funding statement:
This research received no external funding.

Conflict of Interest:
The authors declare that they have no conflict of interest.

AI Statement:
During the preparation of this work the author used check spelling tools in order to grammar correct. After using this tool, the author reviewed and edited the content as needed and takes full responsibility for the content of the publication.

Author Contributions:
All authors contributed to the study conception and design. Material preparation, data collection, and analysis ... were performed by M. R., A. R., and H. Z. The first draft of the manuscript was written by M. R., A. R., and H. Z. The author reads and approved the final manuscript.

References
1. Suerich-Gulick F, Gaskin SJ, Villeneuve M, Parkinson É. Characteristics of free surface vortices at low-head hydropower intakes. Journal of Hydraulic Engineering. 2014 Mar 1;140(3):291-9. https://doi.org/10.1061/(ASCE)HY.1943-7900.0000826
2. Knauss J, editor. Swirling flow problems at intakes. Routledge; 2017 Nov 1.
3. Rankine WJ. A manual of applied mechanics. C. Griffin and Company, Limited; 1901.
4. Hecker GE, editor. Fundamentals of vortex intake flow. IAHR hydraulic structures design manual. Rotterdam: Balkema, [chapters 2 and 8]. 1987.
5. Sarkardeh H, Zarrati AR, Roshan R. Effect of intake head wall and trash rack on vortices. Journal of Hydraulic Research. 2010 Feb 1;48(1):108-12. https://doi.org/10.1080/00221680903565952
6. White F. Fluid Mechanics (5th ed.). New York, NY: McGraw-Hill. 2003.
7. Travis QB, Mays LW. Prediction of intake vortex risk by nearest neighbors modeling. Journal of Hydraulic Engineering. 2011 Jun 1;137(6):701-5. https://doi.org/10.1061/(ASCE)HY.1943-7900.0000344
8. Heravi Z, Azhdary Moghaddam M, Esmaili K, Givehchi M, Bahr Peyma A. Experimental Evaluation of Performance of the New Design of Bed Protection Models (F-jacks) in Altering the Flow Pattern around Bridge Piers. Journal of Hydraulics. 2024 Mar 20;19(1):67-86. https://doi.org/10.30482/jhyd.2023.395247.1643
9. Camnasio E, Orsi E, Schleiss AJ. Experimental study of velocity fields in rectangular shallow reservoirs. Journal of Hydraulic Research. 2011 Jun 1;49(3):352-8. https://doi.org/10.1080/00221686.2011.574387
10. Sarkardeh H, Jabbari E, Zarrati AR, Tavakkol S. Velocity field in a reservoir in the presence of an air-core vortex. InProceedings of the Institution of Civil Engineers-Water Management 2014 Jun;167(6):356-64. Thomas Telford Ltd. https://doi.org/10.1680/wama.13.00046
11. Mulligan S, Casserly J, Sherlock R. Effects of geometry on strong free-surface vortices in subcritical approach flows. Journal of Hydraulic Engineering. 2016 Nov 1;142(11):04016051. https://doi.org/10.1061/(ASCE)HY.1943-7900.0001194
12. Naderi V, Gaskin S. A 3D study of an intake air-core vortex structure using PIV & flow visualization. In: Proc of 7th International Symposium on Hydraulic Structure. 2018: Aachen, Germany.
13. Naderi V, Farsadizadeh D, Lin C, Gaskin S. A 3D study of an air-core vortex using HSPIV and flow visualization. Arabian Journal for Science and Engineering. 2019 Oct;44(10):8573-84. https://doi.org/10.1007/s13369-019-03764-3
14. Duinmeijer A, Oldenziel G, Clemens F. Experimental study on the 3D-flow field of a free-surface vortex using stereo PIV. Journal of Hydraulic research. 2020 Jan 2;58(1):105-19. https://doi.org/10.1080/00221686.2018.1555558
15. Hamidi, S., Sarkardeh, H., Bashtani, A. Spiral Flow Measurement at Vertical Intakes Using PTV Method. Journal of Hydraulic Structures, 2024; 11(1): 41-50. doi: 10.22055/jhs.2024.47215.1304

16. Azarpira M, Sarkardeh H, Tavakkol S, Roshan R, Bakhshi H. Vortices in dam reservoir: A case study of Karun III dam. Sadhana. 2014 Oct;39(5):1201-9. https://doi.org/10.1007/s12046-014-0252-7
17. Amiri SM, Zarrati AR, Roshan R, Sarkardeh H. Surface vortex prevention at power intakes by horizontal plates. InProceedings of the institution of civil engineers-water management 2011 Apr;164(4):193-200. Thomas Telford Ltd. https://doi.org/10.1680/wama.1000009
18. Khanarmuei M, Rahimzadeh H, Sarkardeh H. Investigating the effect of intake withdrawal direction on critical submergence and strength of vortices. Modares Mechanical Engineering. 2015;14(10):35-42.
19. Khanarmuei MR, Rahimzadeh H, Kakuei AR, Sarkardeh H. Effect of vortex formation on sediment transport at dual pipe intakes. Sādhanā. 2016 Sep;41(9):1055-61. https://doi.org/10.1007/s12046-016-0531-6
20. Khanarmuei M, Rahimzadeh H, Sarkardeh H. Effect of dual intake direction on critical submergence and vortex strength. Journal of Hydraulic Research. 2019 Mar 4;57(2):272-9. https://doi.org/10.1080/00221686.2018.1459896
21. Monshizadeh M, Tahershamsi A, Rahimzadeh H, Sarkardeh H. Comparison between hydraulic and structural based anti-vortex methods at intakes. The European Physical Journal Plus. 2017 Aug 3;132(8):329. https://doi.org/10.1140/epjp/i2017-11608-4
22. Monshizadeh M, Tahershamsi A, Rahimzadeh H, Sarkardeh H. Vortex dissipation using a hydraulic-based anti-vortex device at intakes. International Journal of Civil Engineering. 2018 Sep;16(9):1137-44. https://doi.org/10.1007/s40999-017-0266-8
23. Taghizadeh A, Sarkardeh H, Azamathulla HM. Mechanisms of free surface vortex formation at water intakes (a review). Dams and Reservoirs. 2025 Sep 11. https://doi.org/10.1680/jdare.25.01007
24. Amini AA, Sarkardeh H, Jabbari E, Eidi A. Understanding vortex characteristics in hydraulic systems: a temperature-driven analysis. Modeling Earth Systems and Environment. 2024 Jun;10(3):3559-71. https://doi.org/10.1007/s40808-024-01969-6
25. Zhang B, Ma L, Cheng L, Zhu B, Qin Y. Characterization of free-surface vortex evolution and its impact on hydraulic stability of the pump sump. Experimental Thermal and Fluid Science. 2025 Jul 1;166:111466. https://doi.org/10.1016/j.expthermflusci.2025.111466
26. Jiao W, Fan H, Xi X, Shen J, Zhou L, Jia X, Wang Z, Cheng L. Study on the key influencing factors and vortex characteristics of the water jet propulsion pump underwater suction vortex. Physics of Fluids. 2025 Sep 1;37(9). https://doi.org/10.1063/5.0287735
27. Mondal RK, Rohilla L, Kumar P. Free surface vortex and associated air entrainment during liquid drainage using two outlets. Experimental Thermal and Fluid Science. 2025 Jan 1;160:111314. https://doi.org/10.1016/j.expthermflusci.2024.111314
28. Roushangar K, Akhgar S, Salmasi F, Shiri J. Modeling energy dissipation over stepped spillways using machine learning approaches. Journal of Hydrology. 2014 Jan 16;508:254-65. https://doi.org/10.1016/j.jhydrol.2013.10.053
29. Ghorbani MA, Salmasi F, Saggi MK, Bhatia AS, Kahya E, Norouzi R. Deep learning under H2O framework: A novel approach for quantitative analysis of discharge coefficient in sluice gates. Journal of Hydroinformatics. 2020 Nov 1;22(6):1603-19. https://doi.org/10.2166/hydro.2020.003
30. Ghorbani MA, Khatibi R, Singh VP, Kahya E, Ruskeepää H, Saggi MK, Sivakumar B, Kim S, Salmasi F, Hasanpour Kashani M, Samadianfard S. Continuous monitoring of suspended sediment concentrations using image analytics and deriving inherent correlations by machine learning. Scientific reports. 2020 May 22;10(1):8589. https://doi.org/10.1038/s41598-020-64707-9
31. Salmasi F, Abraham J. Expert system for determining discharge coefficients for inclined slide gates using genetic programming. Journal of Irrigation and Drainage Engineering. 2020 Dec 1;146(12):06020013. https://doi.org/10.1061/(ASCE)IR.1943-4774.0001520
32. Salmasi F, Sihag P, Abraham J, Nouri M. Experimental investigation and prediction of free fall jet scouring using machine learning models. International Journal of Sediment Research. 2023 Jun 1;38(3):405-20. https://doi.org/10.1016/j.ijsrc.2022.11.004

33. Anwar HO, Weller JA, Amphlett MB. Similarity of free-vortex at horizontal intake. Journal of Hydraulic Research. 1978 Apr 1;16(2):95-105. https://doi.org/10.1080/00221687809499623
34. Liu FT, Ting KM, Zhou ZH. Isolation forest. In2008 eighth ieee international conference on data mining 2008 Dec 15 (pp. 413-422). IEEE. https://doi.org/10.1109/ICDM.2008.17
35. Manevitz LM, Yousef M. One-class SVMs for document classification. Journal of machine Learning research. 2001;2(Dec):139-54.
36. Bushra AA, Yi G. Comparative analysis review of pioneering DBSCAN and successive density-based clustering algorithms. IEEE Access. 2021 Jun 14;9:87918-35. https://doi.org/10.1109/ACCESS.2021.3089036
37. Cea L, Puertas J, Pena L. Velocity measurements on highly turbulent free surface flow using ADV. Experiments in fluids. 2007 Mar;42(3):333-48. https://doi.org/10.1007/s00348-006-0237-3

© 2025 by the authors. Licensee SCU, Ahvaz, Iran. This article is an open access article distributed under the terms and conditions of the Creative Commons Attribution 4.0 International (CC BY 4.0 license) (http://creativecommons.org/licenses/by/4.0/).

Appendix A. Derivation of the Inverse Muskingum Routing Equation with Lateral Flow

Discretizing Eq. (1) over a time interval Δt using a weighted scheme gives:

$$\frac{S_2 - S_1}{\Delta t} = (1+\beta)[(1-\theta)I_1 + \theta I_2] - [(1-\theta)O_1 + \theta O_2] \tag{A1}$$

The storage values at the beginning and end of the time step are obtained from Eq. (2):

$$S_2 = K[X(1+\beta)I_2 + (1-X)O_2] \tag{A2}$$
$$S_1 = K[X(1+\beta)I_1 + (1-X)O_1] \tag{A3}$$

Substituting Eqs. (A2) and (A3) into Eq. (A1) and rearranging terms yields:

$$\frac{K[X(1+\beta)I_2 + (1-X)O_2] - K[X(1+\beta)I_1 + (1-X)O_1]}{\Delta t} = (1+\beta)[(1-\theta)I_1 + \theta I_2] - [(1-\theta)O_1 + \theta O_2] \tag{A4}$$

Solving for the unknown upstream inflow I_1 results in the inverse routing equation:

$$I_1 = C_1 O_2 + C_2 O_1 + C_3 I_2 \tag{A5}$$

where the coefficients are defined as:

$$C_1 = \frac{1}{1+\beta}\frac{K(1-X) + \theta\Delta t}{KX + (1-\theta)\Delta t}$$
$$C_2 = \frac{-1}{1+\beta}\frac{K(1-X) - (1-\theta)\Delta t}{KX + (1-\theta)\Delta t} \tag{A6}$$
$$C_3 = \frac{KX - \theta\Delta t}{KX + (1-\theta)\Delta t}$$

This formulation enables inverse flood routing while explicitly accounting for lateral flow contributions through the parameter β.